European Journal of Nuclear Medicine and Molecular Imaging
https://doi.org/10.1007/s00259-019-04630-y

ORIGINAL ARTICLE

Digital versus analogue PET in [^{68}Ga]Ga-PSMA-11 PET/CT for recurrent prostate cancer: a matched-pair comparison

Ian Alberts[1] · George Prenosil[1] · Christos Sachpekidis[1] · Thilo Weitzel[1] · Kuangyu Shi[1] · Axel Rominger[1] · Ali Afshar-Oromieh[1]

Received: 20 September 2019 / Accepted: 18 November 2019

Abstract

Purpose Digital PET/CT scanners represent a significant step forward in molecular imaging. We report here the clinical impact of digital PET in PSMA-PET/CT.

Methods In this retrospective study, 88 consecutive patients who underwent [^{68}Ga]Ga-PSMA-11 PET/CT on a digital PET/CT (dPET/CT) scanner for recurrent prostate cancer (PC) were included in a first cohort. In a second step, 88 individuals who underwent an analogue [^{68}Ga]Ga-PSMA-11 PET/CT (aPET/CT) were selected after they were matched to the first cohort for clinical parameters. Following consensus read by two nuclear medicine physicians, the number and type of PC lesions as well as benign, PSMA-positive lesions were recorded. The results were complemented by extensive [^{68}Ga]Ga phantom measurements to determine imaging characteristics of both scanners.

Results dPET/CT revealed a greater number of PC lesions compared to aPET/CT (326 versus 142) as well as a proportional increase in benign causes of tracer-uptake (144 versus 65). A greater number of scans were noted as pathological for PC on dPET/CT (74/88) compared to aPET/CT (64/88, $p < 0.05$). The PSMA positivity rate for PC was significantly higher in dPET/CT for the lowest PSA values (PSA < 2.0 ng/ml, $p < 0.05$).

Conclusion dPET/CT detected more PC lesions compared to aPET/CT. A significantly higher rate of pathological PET/CTs was noted in the group with the lowest PSA values. A higher number of benign PSMA-positive lesions were also noted in dPET/CT. The differences could be plausibly explained by the measured imaging characteristics of the scanners.

Keywords Prostate cancer · PET/CT · Positron emission tomography · PSMA · Prostate-specific membrane antigen · Digital PET

Introduction

Prostate cancer (PC) is the most common malignancy in men and the third leading cause of cancer-related death in men [1]. Despite initial therapy at early-stage disease, biochemical recurrence remains a commonly encountered entity and presents a challenge for conventional imaging modalities given their limited abilities to detect disease at early stages of recurrence. Although the exact timing of salvage radiotherapy (SRT) remains a topic of debate, early SRT may be beneficial for some patients [2]. However, previous studies have demonstrated that at lower PSA values (and therefore at early-stage biochemical recurrence), the diagnostic performance of PSMA ligands remains limited [3]. The challenge for nuclear medicine is therefore to develop methods better suited to the detection of PC recurrence at early stage.

The prostate-specific membrane antigen (PSMA), also known as folate hydrolase I or glutamate carboxypeptidase II, has become the focus of much attention owing to its high levels of expression on PC cells [4]. Following its clinical introduction in 2011, PSMA ligand molecular imaging has rapidly established itself as the investigation of choice in recurrent PC [3, 5–7]. Furthermore, PSMA-directed radioligand therapy is a rapidly evolving treatment modality for metastatic disease, creating an additional theragnostic role for PSMA ligand molecular imaging [8]. A number of PSMA-

This article is part of the Topical Collection on Oncology – Genitourinary

Electronic supplementary material The online version of this article (https://doi.org/10.1007/s00259-019-04630-y) contains supplementary material, which is available to authorized users.

✉ Ian Alberts
ian.alberts@insel.ch

[1] Department of Nuclear Medicine, Inselspital, Bern, Switzerland

Published online: 02 December 2019

radioligands have become available to the nuclear medicine physician and are the result of a concerted research effort in recent years to develop tracers best suited for the identification of PC lesions.

In step with these recent advances in radiopharmacy, there has been much recent progress in PET/CT technology. Since the introduction of the first combined PET/CT scanner in 2000 [9], PET detectors have been based on scintillation crystals coupled with photomultiplier tubes (PMT), which introduces inherent physical limitations to the scanner's performance. The recent introduction by several manufacturers of new-generation fully digital PET/CT (dPET/CT) systems based on solid state detectors represents a significant step forward in this regard, with a number of technical advantages including 1:1 coupling between crystals and detectors, enhanced spatial resolution, faster TOF and shorter dead time. Initial reports for various systems demonstrate favourable performance characteristics in comparison to previous generation analogue systems [10–12], which correlate to improvement in image quality [13] and lesion detection [14]. However, whether such technical performance characteristics translate into a higher detection rate in PSMA-PET/CT has not been demonstrated, which this paper aims to address. We also provide head-to-head phantom measurements for ^{68}Ga which provide an objective basis upon which to interpret our clinical findings.

Materials and methods

Patient population

In this retrospective analysis, we included 88 individuals who were examined on our digital PET/CT (dPET/CT) between October 2018 and March 2019. On the basis of PSA and Gleason Score, 88 corresponding patients examined between February 2018 and October 2018 on one of two cross-calibrated analogue PET/CT scanners (aPET/CT) were included, with age and tumour stage (T, N and M) as closely matched as possible. Previous treatments are outlined in Table 1.

Table 1 Details of initial treatment of both cohorts. *OP* operative (prostatectomy), *OP + RT* combined prostatectomy and radiotherapy, *RT* radiotherapy alone, *Chemo* chemotherapy; *Unknown* details of initial treatment not available in patients' notes. N.B. all patients receiving ADT were excluded from this study

Initial treatment(n)	Digital (*n* =)	Analogue (*n* =)
OP	55	56
OP + RT	10	20
RT	14	10
Chemo	1	0
Unknown	8	2

The patients were then grouped by PSA value (<0.5, 0.5–2.0, 2.0–4.0, >4.0 ng/ml). Both cohorts' characteristics are outlined in Table 2. All patients were referred to our centre for [^{68}Ga]Ga-PSMA-11-PET/CT in the setting of biochemically recurrent PC. Any patients with androgen deprivation therapy in the previous 6 months were excluded, given the known influence this has on PSMA expression [15].

All patients provided written, informed consent for anonymous retrospective evaluation of their clinical information, which was performed in accordance with the Helsinki Declaration. This retrospective study was approved by the institutional ethics commission (KEK-Nr. 2018-00299).

Radiotracer

[^{68}Ga]Ga-PSMA-11 was produced as previously described [7, 16]. The [^{68}Ga]Ga-PSMA-11 solution given by intravenous

Table 2 Matched-pair cohort characteristics [median (min-max)] for each PSA group: Gleason Score (GS), Age und TNM Stage (Union for International Cancer Control UICC, 8th Ed.)

PSA < 0.5 ng/mL		
	Digital	Analogue
GS	7 (7–9)	7 (6–9)
Age	70 (57–77)	67 (58–76)
T	3 (0–3)	2 (2–3)
N	0 (0–1)	0 (0–1)
M	0	0
PSA 0.5–2.0 ng/mL		
	Digital	Analogue
GS	7 (6–9)	7 (6–9)
Age	67 (50–78)	67 (58–78)
T	3 (1–3)	3 (2–3)
N	1 (0–1)	0 (0–1)
M	0	0
PSA 3.0–4.0 ng/mL		
	Digital	Analogue
GS	7 (6–9)	7 (6–9)
Age	72 (54–83)	72 (55–83)
T	3 (1–4)	2 (2–3)
N	0 (0–1)	0 (0–1)
M	n = 1	0
PSA 3.0–4.0 ng/mL		
	Digital	Analogue
GS	7 (6–9)	7 (6–9)
Age	71 (48–83)	71 (54–78)
T	2 (1–4)	3 (1–3)
N	0 (0–1)	1 (0–1)
M	n = 3	n = 0

bolus injection (for the dPET/CT mean of 218 ± 31 MBq, range 162−312 MBq; for the aPET/CT mean 197 ± 18 MBq, range 124−222) with a target dose of 3 MBq/kg.

Imaging

All patients received regular whole-body PET scans (from head to the thighs) at 1.5 h p.i following oral hydration with 1 L of water (beginning from 30 min p.i.) and 20 mg of i.v. furosemide (at 1 h p.i.).

Image acquisition

All patients were investigated using either a Biograph-VISION 600 PET/CT digital scanner (n = 88) "dPET/CT" or one of two cross-calibrated Biograph-mCT PET/CT analogue scanners (n = 88) ("aPET/CT") (both: Siemens, Erlangen, Germany). The examination protocols and reconstruction algorithms used are included in supplementary materials I.

Image evaluation

Image analysis was performed using an appropriate workstation and software (SyngoVia; Siemens, Erlangen, Germany). Two experienced physicians (one postgraduate physician with 7 years' clinical experience and one board-certified nuclear physician with 10 years' experience – first and third authors, respectively) read the data sets together and resolved any disagreements by consensus.

Lesions that were visually considered at consensus read as suggestive for PC exhibiting increased tracer-uptake relative to local background were counted. The examination was noted to be "positive" (pathologic) or "negative" for PSMA-avid PC lesions.

For calculation of the maximum standardised uptake value (SUVmax), circular regions of interest were drawn around areas with focally increased uptake in transaxial slices and automatically adapted to a three-dimensional volume of interest at a 40% isocontour as previously described [7]. Lesion to background ratio (TBR) was determined by measurement of SUVmax relative to the mean standardised uptake value (SUVmean) of a 1 cm^3 volume of interest (VOI) placed in the left gluteal musculature. SUVmax for lesion suggestive of PC and SUVmean for gluteal uptake were chosen as the values with the lowest coefficient of variation [17]. Cross-sectional area was determined by orthogonally placed diameter measurements for the largest cross-sectional diameter as determined by the co-registered CT.

Lesions identified by consensus as benign structures such as ganglia, ureteric activity or nonspecific tracer-uptake associated with clearly identifiable benign structures such as bone fractures were counted. Visual criteria for the differentiation between ganglia and lymph nodes were as described previously [18] and aided by a co-registered thin-slice CT (CT parameters in supplementary materials). Known pitfalls were considered according to previously published criteria [18–20].

Statistical analysis

Statistical analyses were performed using Excel (Microsoft, Redmond, Washington). Comparison in detection rates for the two matched-pair cohorts was calculated by Pearson's chi-squared test. P values < 0.05 were considered statistically significant. Differences in the means for lesion SUVmax, TBR and cross-sectional diameter were determined by the unpaired t-test (two-tailed).

Phantom measurements

Six water-filled active spheres with volumes of 0.25 ml, 0.5 ml, 1 ml, 2 ml, 4 ml and 8 ml were filled with ^{68}Ga-PSMA-11 and circularly arranged in cylindrical phantom of 220 mm diameter filled with 6830 ml of active water background. Sphere walls consisted of 1-mm-thick epoxy resin, and the spheres were mounted on a 4-mm-thick and 40-mm-long epoxy rod. The radial offset of the spheres was 70 mm, and the ratio of foreground (sphere) activity concentration (FAC) to background activity concentration (BAC) was five to one. The same phantom was used consecutively on both examined PET/CT systems, with the initial sphere activity being 28.1 kBq/ml at the beginning of the digital PET measurements and 13.3 kBq at the beginning of the analogue PET measurements. Please note that the custom-made metric spheres are smaller than the NEMA NU2 spheres commonly used for PET calibration. Additionally, the spheres' variation in volume is more regular and more densely sampled in comparison to NEMA NU2 standards. Consequently, the according phantom measurements more closely match the actual clinical imaging situation under investigation. Moreover, phantom measurements on each scanner comprise 16 differing acquisition times covering a broad range of possible exposures and according signal-to-noise ratios. Further acquisition details can be found in supplementary materials II.

Results

Detection rate

As shown in Fig. 1, a higher number of lesions were identified by dPET/CT compared with aPET/CT (benign,144 versus 65; PC lesions 326 versus 142), and a significantly higher number of individuals (74/88, 84%) had pathological PSMA-PET by dPET/CT, compared to aPET/CT (64/88, 73% p = 0.0476).

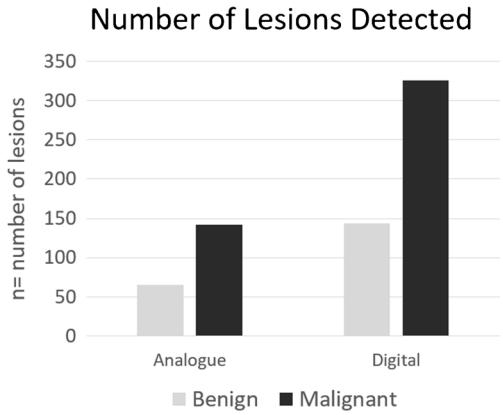

Fig. 1 Number of both benign and malignant lesions detected by analogue and digital PET/CT in the patient cohorts

Figure 2 shows the PET positivity rate by PSA group. Notably, statistically significant higher rates ($p = 0.01$) were noted for the PSA < 0.5 ng/ml group and the PSA 0.5–2.0 ng/ml group ($p = 0.01$). For PSA values > 2.0, no statistically significant difference was noted. We also note that the asymptote (beyond which no significant increase is seen) was achieved at PSA 0.5–2.0 ng/ml for dPET/CT and PSA 2.0–4.0 ng/ml for aPET/CT, suggesting that the maximal rate of pathological PSMA/PET is reached at earlier PSA values in dPET/CT compared with aPET/CT.

Detection by lesion type

Lesions were classified as benign, lymph node metastasis (LN) of PC, bone metastasis of PC or local recurrence (in the prostatic fossa or seminal vesicles). No patterns were discernible in the comparison between dPET/CT and aPET/CT, with roughly proportional patterns observed between the two cohorts. The results are shown in Fig. 3.

Lesion size, SUVmax and lesion to background ratio

For the PSA groups in which differences were discernible for the detection rate (PSA < 0.5 and PSA 0.5–2.0 ng/ml), a subanalysis was then performed for lesion size, lesion SUVmax and lesion to background ratio. No statistically significant differences in lesion size were noted between the two cohorts. We note lower, albeit nonsignificant SUVmax values for PC lesions on dPET/CT at PSA < 0.5 ng/ml, with statistical significance being reached for the PSA 0.5–2.0 ng/ml group. Likewise, for tumour-to-background ratio (TBR), higher, albeit nonsignificant TBR values were observed for dPET/CT at PSA < 0.5, with statistical significance being reached for the PSA 0.5–2.0 ng/ml group ($p = 0.03$). The results are shown in Table 3.

Follow-up

To interrogate the possibility that the higher detection rate for the dPET/CT was a result of the incorrect identification of PSMA-avid lesions (i.e. false positives) clinical follow-up was performed. In particular, for the patients where a higher detection rate was noted, patient notes were interrogated for correlative information. For dPET/CT patients in the PSA < 0.5 ng/ml and 0.5–2.0 ng/ml cohorts, clinical follow-up was available for 65% of patients ($n = 22/34$). Of those for whom follow-up was available, 81.8% ($n = 18$) went on to receive radiotherapy, 9.1% ($n = 2$) chemotherapy, 4.5% ($n = 1$) hormone deprivation and 4.5% ($n = 1$) watchful waiting. All patients with posttreatment PSA values available ($n = 9$) had a fall in PSA, with none presenting with rising or equivocal results. For those without PSA values available, a further ($n = 6$) patients had correlative MRI findings. No examples of discordant imaging were noted. For the remaining $n = 7$ patients, regrettably no correlative findings were available.

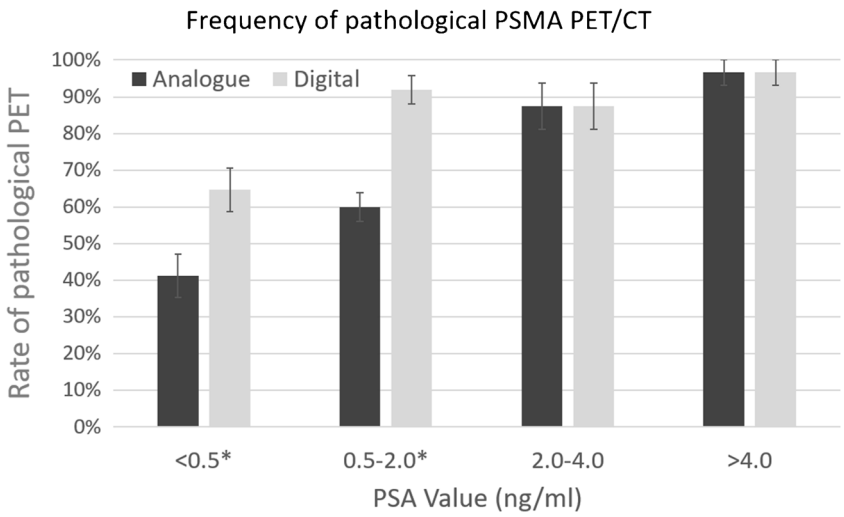

Fig. 2 Frequency of pathological PSMA-PET/CT by scanner type and PSA group. *Indicates groups where statistical significance was reached (PSA < 0.5 and PSA 0.5–2.0)

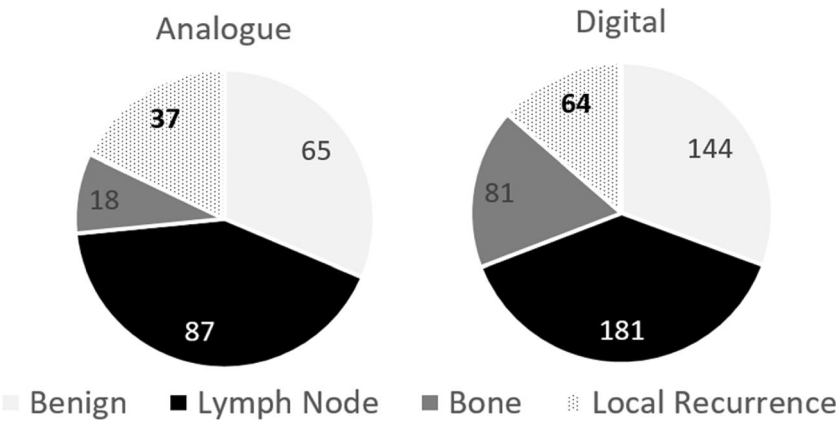

Fig 3 Largely proportional patterns of lesions were identified across both cohorts

Phantom measurements

Figure 4 a and b show normalised recovery values plotted against exposure for both scanner types, dPET/CT and aPET/CT. The expected recovery for each sphere is seen at the highest exposures, with normalised recovery values being higher for smaller spheres in dPET/CT. For example, in the case of the 0.25-ml sphere, recovery amounted to 0.33 for aPET/CT and 0.57 for dPET/CT.

Decreasing exposure and thus decreasing the image count statistics lead to apparently increasing recovery values. This excess in recovery was more pronounced in data from dPET/CT, where up to a factor of 2.5 versus a factor of 1.5 higher recovery was observed in contrast to aPET/CT.

Figure 4 c and d show the distinguishability of the spheres (foreground) against their background, which is illustrated by the vertical lines (which represent the intersection between the background and sphere activity). Further details on the mathematical definition are detailed in supplementary materials II.

The 10% quantiles estimated for the 0.25-ml sphere intersected the noise 90% quantiles at an exposure of 124 kDecays/ml in aPET/CT and at 21 kDecays/ml in dPET/CT. The intersection for the 0.5-ml sphere in aPET/CT happened at 35 kDecays/ml, whereas for this sphere, no intersection could be seen in dPET/CT. All other spheres showed no intersections between quantiles. This proves that smaller spheres are better distinguishable from background in dPET/CT at low exposures. At this point, we note that the coefficient of variation of the background activity concentration was the same for both PET/CT systems over the entire exposure range (dashed lines).

In Fig. 4c and d, we fitted a power law function to the recovery exposure curves from Fig. 4a and b. This shows more clearly the transition of the recovery from a constant value at high exposures to a steeply rising value at low exposures, a measure of image noise. We see that this transition occurs at higher exposures for aPET/CT compared with dPET/CT, again illustrating the improved contrast-to-noise ratio (CNR) in the latter. This is further supported by the log-log plot for the CNR versus exposure (Fig. 5). Here, the CNR was better over the entire exposure range for dPET/CT than for aPET/CT.

Table 3 Comparison of lesion characteristics between two scanner types (lesion size, SUVmax of pathological lesions and tumour/background ratio). All data presented as mean ± standard deviation (minimum-maximum). Instances where results reach statistical significance are marked by an asterisk*

Size of PC lesions (cross-sectional diameter (cm)			
PSA	Digital	Analogue	p
<0.5	1.2 ± 1.4(0.36–7.74)	1.05 ± 1.0(0.3–5.6)	p = 0.74
0.5–2.0	0.9 ± 0.39(0.26–2.75)	1.05 ± 0.74(0.4–4.6)	p = 0.25
PC Lesion SUVmax			
PSA	Digital	Analogue	p
<0.5	9.7 ± 6.0(3.3–28)	11.1 ± 7.6(4.1–28.8)	p = 0.36
0.5–2.0	6.7 ± 5.6(1.6–18.2)	11.0 ± 18.9(2.1–41.9)	p = 0.11
Tumour/background ratio			
PSA	Digital	Analogue	p
<0.5	33.6 ± 21.6(12.3–93.3)	22.4 ± 37.4(10.3–128.0)	p = 0.36
0.5–2.0	41.0 ± 33.9(8.0–114.0)	31.4 ± 35.1(5.3–134.0)	p = 0.030

Discussion

As described, PET/CT with PSMA-targeted radioligands has rapidly become the investigation of choice in recurrent PC, exhibiting impressive diagnostic performance, and several recent publications demonstrate their outperformance of conventional imaging techniques such as MRI [21, 22]. Nevertheless, early stages of recurrence continue to represent a significant diagnostic challenge. While prospective studies are yet to confirm the clinical benefit of early PSMA-guided radiotherapy [23], the challenge remains for nuclear medicine physicians to accurately diagnose recurrent PC at earlier stages where the chance for a curative therapy may be at its highest.

The recent introduction by several manufacturers of digital PET/CT scanners onto the market represents a

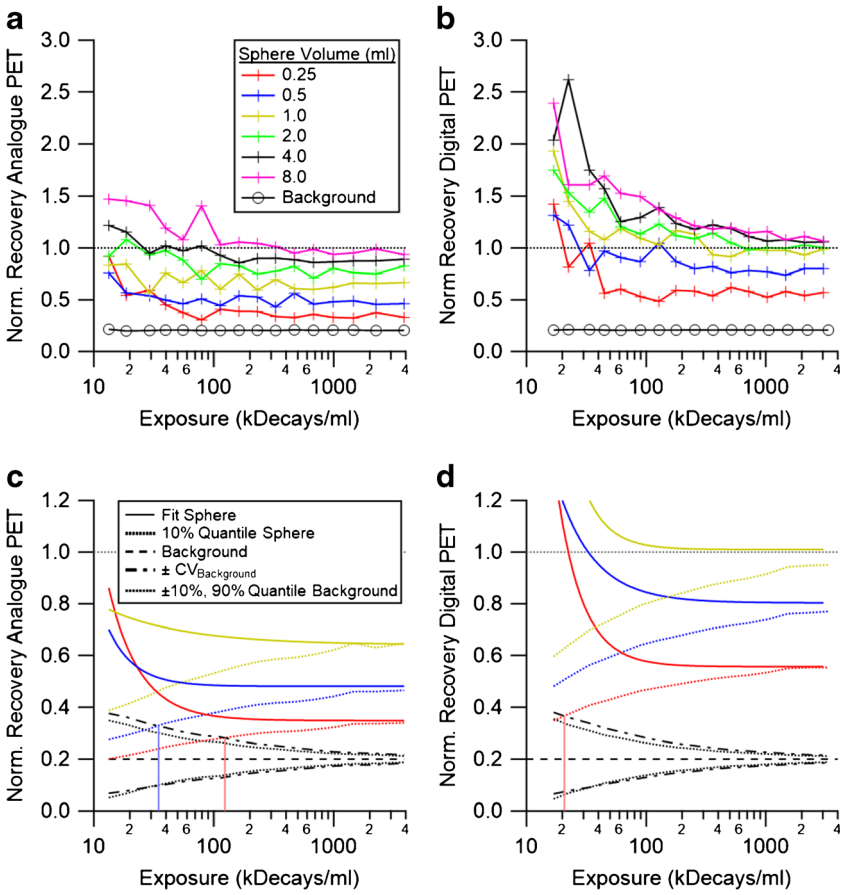

Fig 4 Normalised recovery of maximal values found in spheres and mean background values plotted against exposure for analogue PET/CT (**a**) and digital PET/CT (**b**). In (**c**) and (**d**), a power law fit is shown instead of the actual measurement points (solid lines). Dotted lines represent the quantiles and the dashed lines represent the background with its coefficient of variation. Vertical lines show intersections between sphere and background quantiles. Colours in legend (**a**) apply to all.

significant development in nuclear medicine. Compared to previous generation analogue scanners, such dPET/CT systems demonstrate very favourable performance characteristics [10, 11] with increased lesion detection, sensitivity and image quality being reported by numerous studies [12, 24]. More recently, Fuentes-Ocampo et al. published an intra-patient analysis in [^{18}F]FDG PET/CT, albeit limited to comparison in SUVmax measurements rather than detection rate [25]. Nguyen et al. also found increased image quality, SUV values and lesion sharpness, with additional lesions being identified in dPET/CT in 5 of their cohort of 21 patients in [^{18}F]FDG PET for oncological patients [12]. Nevertheless, these studies limit themselves to lesion-based analyses and have been performed in small cohorts. López-Mora et al. report improved image quality, inter-reader agreement and no significant difference in the total number of lesions detected by each system. They did, however, note an improved lesion detection for a small subset of patients in a prospective head-to-head series of 100 patients using [^{18}F]-FDG or

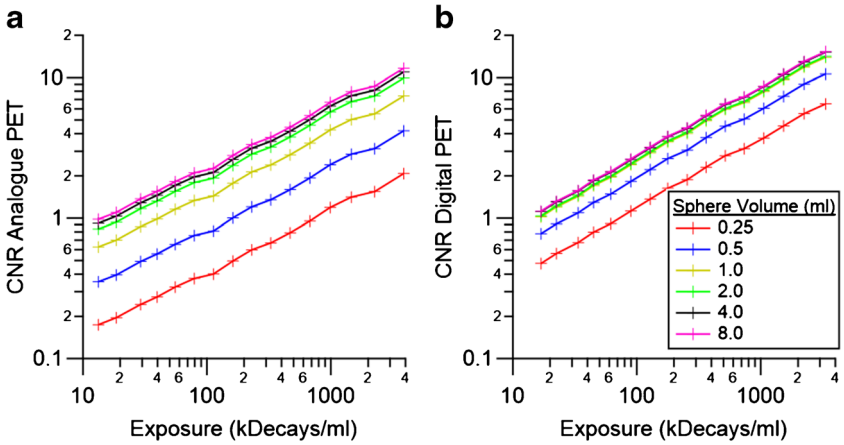

Fig 5 Contrast-to-noise ratios (CNR) for analogue PET/CT (**a**) and digital PET/CT (**b**) plotted against exposure

[^{18}F]-FluoroCholine [14]. However, no publications report the clinical impact of dPET/CT PSMA-PET/CT, which this study aims to address.

Fuentes-Ocampo et al. randomly assigned patients to dPET/CT with repeat scanning by aPET/CT on the same day and vice-versa [25]. While this methodology afforded an elegant lesion-based comparison, we do not consider this approach well suited to PSMA-PET/CT, where a combination of short radioisotope half-life and in vivo tracer-kinetics means that repeat scanning would have to be performed at a separate occasion with comparable tracer-uptake time, resulting in an unjustifiable additional radiation exposure [26, 27]. Instead, we propose a matched-pair approach, as previously published for the comparison of PSMA-radioligands [28].

In contrast to López-Mora et al., who report no increased total lesion detection in dPET/CT, our retrospective matched-pair analysis revealed a higher detection rate for PSMA-avid PC lesions in dPET/CT compared to aPET/CT, with more than twice as many lesions detected in dPET/CT (326 versus 142) [14]. A proportional increase in PSMA-avid benign lesions was also noted (144 versus 65). Consequently, a higher overall PSMA positivity rate was noted in dPET/CT (an extra 10 patients, 11%). Division of the patients into PSA groups (PSA < 0.5, PSA 0.5–2.0, PSA 2.0–4.0 and PSA > 4.0 ng/ml) revealed a statistically significant higher rate of pathological PET for the lowest PSA groups (PSA < 0.5 and 0.5–2.0) demonstrating the utility of dPET/CT in the diagnostically most challenging groups. Our PSMA positivity rate in aPET/CT was comparable to those previously published for the same tracer and comparable examination protocol [3].

We note that beyond certain PSA values, no increase is to be expected, with a maximum detection rate of 97%; a small number of dedifferentiated PC lesions exhibit no PSMA-avidity meaning that 100% cannot be achieved [29]. It is apparent that the rate of pathological PET rises with PSA until a certain value, beyond which no further increase occurs. The asymptote for this is observed to occur at lower PSA values in dPET/CT (PSA 0.5-2.0 ng/ml) compared with aPET/CT (2.0–4.0 ng/ml). Beyond these values, no difference between the two scanners was observed. We interpret this finding as being of substantial clinical value: hitherto our institutional advice in the case of initially negative PSMA scanning is to repeat imaging at PSA > 2.0 ng/ml, and should this subsequent scan be negative, we recommend [^{18}F]F-Choline PET to rule out non-PSMA-avid disease. In the light of these results, we suggest this threshold be lowered in the case of dPET/CT. Furthermore, when selecting patients for imaging, those presenting with PSA values <2.0 ng/ml should be directed to dPET/CT when available.

In common with studies in recurrent PC, no histological verification of our lesion classification was available. In order to mitigate against this, we considered known pitfalls and causes of benign uptake (such as ganglia or degenerative/benign bone disease) at a consensus reading of all scans [18–20, 30, 31]. Cognisant of the possibility that the increased detection rate observed could be attributable to increased non-specific tracer-uptake and subsequent misidentification of lesions, we undertook clinical follow-up for the subset of dPET/CT patients at PSA < 2.0 ng/ml. Follow-up information was available for 65% of this subgroup of patients, a favourable rate compared with previous matched-pair analyses [28]. For all patients with available follow-up, either concordant falls in post-radiotherapy PSA or correlative MRI imaging was available, with no discordant cases noted.

We also note with interest the increased rate of benign PSMA uptake reported in [^{18}F]-based PSMA ligands, such as [^{18}F]-PSMA-1007 [28, 32], whereas any increase seen in dPET/CT was proportional (see Fig. 3). With the increasing clinical use of such tracers, we expect our finding of proportional increases in benign PSMA uptake to be of even greater significance. Mindful of the fact that studies (which report scanner characteristics) for these tracer-types have hitherto been published using aPET/CT, we consider further studies combining these new tracers with dPET/CT to be of utmost importance.

We also performed sub-analysis of the data with respect to lesion size. Numerous publications have reported detection of smaller lesions owing to the greater spatial resolution afforded by dPET/CT design [11, 33]. Intriguingly, we find no statistically significant difference in lesion size between the dPET/CT and aPET/CT, suggesting that the increased detection rate is not attributable simply to the detection of smaller lesions. Previously published lesion-based SUV analyses reveal higher SUV measurements in the same lesion in dPET/CT [25]. In contrast, our matched-patient cohort analysis revealed that the mean SUVmax lesion was lower in dPET/CT for PSA < 0.5, with statistical significance for PSA 0.5–2.0 and higher tumour-to-background ratio. Noting the higher sensitivity and TBR (tumour-to-background ratio) in dPET/CT, which is confirmed by our extensive phantom measurements, we posit that dPET/CT was better able to detect lesions with lower SUV values. This hypothesis finds support in our clinical observation that this higher detection rate was noted in the lowest PSA group, which can be expected to exhibit weaker PSMA expression [7] and therefore lower tracer-uptake.

Our clinical results find additional support in our phantom measurements, which provides a direct comparison of the two scanners' performance characteristics and complements our matched-pair analysis. Comparing the PET recovery curves obtained from these measurements (Fig. 4a, b), we find higher recovery at the highest exposures for all spherical volumes, reflecting the known higher spatial resolution of the dPET/CT system. When looking at Fig. 4 c and d, we see identical coefficients of variation for the background (CV_{bac}), even

though the spatial resolution of the dPET/CT acquisitions is higher.

This means that any potential increase in image noise brought by an increased spatial resolution was counteracted by the dPET/CT's higher sensitivity. Thus starting at an initial higher recovery, intersections between background and sphere (foreground) activity concentration quantiles occurred at lower exposures or not at all in dPET/CT. Taken together, this reflects an improved contrast-to-noise ratio (CNR) for dPET/CT compared with aPET/CT (as demonstrated in Fig. 5). In clinical terms, this means that dPET/CT is better able to reveal lesions with lower activity concentrations, further supporting our finding that dPET/CT was able to detect lesions characterised with lower SUVmax (Table 3). Furthermore, we hypothesise that the higher tumour-to-background ratio in dPET/CT is a consequence of the system's higher contrast-to-noise ratio (CNR).

In addition to the clinical relevance our results find, namely, that dPET/CT demonstrates a higher rate of pathological PSMA-PET at low PSA values, our results raise important caveats when comparing data quantitatively between different PET/CT systems, an issue first raised by Fuentes-Ocampo et al. [25].

Moreover, we see a higher recovery for large spheres at low exposures in dPET/CT (Fig. 4b). Because of the greater likelihood of encountering higher SUVmax in structures with a greater number of voxels, the higher voxel count in dPET/CT will favour higher SUVmax even at otherwise comparable uptake and noise levels [34], raising further caveats when quantitatively comparing data obtained in different PET/CT systems. Our combined results suggest variability of clinical results as a result of a complex interaction of scanner properties. With new devices being introduced to the market with new technical features and reconstruction algorithms, this variability can be expected to increase. The resultant impact upon variability of clinical results will have to be considered by future publications.

Beyond those already acknowledged, we note additional weaknesses in our study. Ideally, post-prostatectomy and post-radiotherapy patients should be analysed separately, rather than in a mixed cohort, as in this study. Our small sample (88 patients in each group) reflects our initial experiences in a new scanner design. This small sample size resulted in a small lesion yield at the lowest PSA group (PSA < 0.5 ng/ml), which resulted in lack of statistical significance for lesion SUVmax and TBR for this group. Prospective studies with larger cohorts are required to confirm these initial findings. We also note that the scanning acquisition parameters and reconstruction algorithms differed between the two scanners and are cognisant of their effects [34]. Instead, we draw attention to the retrospective methodology, which reflects routine clinical experience, with parameters and reconstruction algorithms tailored to each scanner's performance characteristics and the manufacturer's recommendations.

Although we cannot entirely rule out selection bias, our matched-pair methodology revealed two comparable cohorts. We also draw attention to the non-overlapping date range for each cohort: no aPET patients were examined during the time frame in which the dPET patients were examined. This eliminated any potential bias the choice of scanner type may have had upon our cohorts.

We recognise that this retrospective study reflects only initial experiences with this new scanner type (at the time of writing, our dPET system has had FDA approval for just over 1 year). We eagerly await the results of the prospective phase II trial, due (at the time of writing) in 2 years' time comparing digital and analogue scanning in PSMA/PET-CT for confirmation of our results (NIH Register: NCT03081767).

Conclusion

In this first study reporting the detection rate for [^{68}Ga]Ga-PSMA-11 in dPET/CT for recurrent PC, we find increased detection rates at the lowest PSA values. A higher total number of PSMA-avid lesions of PC were identified in dPET/CT, with a proportional increase in benign causes of PSMA uptake. Our results suggest that the combination of [^{68}Ga]Ga-PSMA-11 and dPET/CT offers increased lesion detection for patients at early stages of recurrence. Sub-analysis of these patients with increased detection rates revealed no difference in size, but rather a lower SUVmax and higher tumour-to-background ratio. In tandem with our phantom measurements performed on both scanners, we find a higher signal-to-noise ratio at lower exposure values, suggesting that the higher detectability in dPET/CT is not solely a result of the higher spatial resolution of the scanner, but rather a result of increased sensitivity for lesions with lower tracer-uptake.

Compliance with ethical standards

Conflict of interest The authors declare that they have no conflict of interest.

Ethical approval All patients published in this manuscript signed a written informed consent form for the purpose of anonymised evaluation and publication of their data. This evaluation was approved by the ethics committee of the University of Bern (KEK-Nr. 2018-00299).

References

1. Siegel RL, Miller KD, Jemal A. Cancer statistics, 2017. CA Cancer J Clin. 2017;67:7–30. https://doi.org/10.3322/caac.21387.
2. Fossati N, Karnes RJ, Colicchia M, Boorjian SA, Bossi A, Seisen T, et al. Impact of early salvage radiation therapy in patients with persistently elevated or rising prostate-specific antigen after radical

prostatectomy. Eur Urol. 2017. https://doi.org/10.1016/j.eururo.2017.07.026.
3. Afshar-Oromieh A, Holland-Letz T, Giesel FL, Kratochwil C, Mier W, Haufe S, et al. Diagnostic performance of 68Ga-PSMA-11 (HBED-CC) PET/CT in patients with recurrent prostate cancer: evaluation in 1007 patients. Eur J Nucl Med Mol Imaging. 2017;44:1258–68. https://doi.org/10.1007/s00259-017-3711-7.
4. Israeli RS, Powell CT, Corr JG, Fair WR, Heston WDW. Expression of the prostate-specific membrane antigen. Cancer Res. 1994;54:1807.
5. Afshar-Oromieh A, Zechmann CM, Malcher A, Eder M, Eisenhut M, Linhart HG, et al. Comparison of PET imaging with a (68)Ga-labelled PSMA ligand and (18)F-choline-based PET/CT for the diagnosis of recurrent prostate cancer. Eur J Nucl Med Mol Imaging. 2014;41:11–20. https://doi.org/10.1007/s00259-013-2525-5.
6. Eiber M, Maurer T, Souvatzoglou M, Beer AJ, Ruffani A, Haller B, et al. Evaluation of hybrid (6)(8)Ga-PSMA ligand PET/CT in 248 patients with biochemical recurrence after radical prostatectomy. J Nucl Med. 2015;56:668–74. https://doi.org/10.2967/jnumed.115.154153.
7. Afshar-Oromieh A, Avtzi E, Giesel FL, Holland-Letz T, Linhart HG, Eder M, et al. The diagnostic value of PET/CT imaging with the (68)Ga-labelled PSMA ligand HBED-CC in the diagnosis of recurrent prostate cancer. Eur J Nucl Med Mol Imaging. 2015;42:197–209. https://doi.org/10.1007/s00259-014-2949-6.
8. Virgolini I, Decristoforo C, Haug A, Fanti S, Uprimny C. Current status of theranostics in prostate cancer. Eur J Nucl Med Mol Imaging. 2018;45:471–95. https://doi.org/10.1007/s00259-017-3882-2.
9. Beyer T, Townsend DW, Brun T, Kinahan PE, Charron M, Roddy R, et al. A combined PET/CT scanner for clinical oncology. J Nucl Med. 2000;41:1369–79.
10. Rausch I, Ruiz A, Valverde-Pascual I, Cal-Gonzalez J, Beyer T, Carrio I. Performance evaluation of the Vereos PET/CT system according to the NEMA NU2-2012 standard. J Nucl Med. 2019;60:561–7. https://doi.org/10.2967/jnumed.118.215541.
11. van Sluis JJ, de Jong J, Schaar J, Noordzij W, van Snick P, Dierckx R, et al. Performance characteristics of the digital Biograph Vision PET/CT system. J Nucl Med. 2019. https://doi.org/10.2967/jnumed.118.215418.
12. Nguyen NC, Vercher-Conejero JL, Sattar A, Miller MA, Maniawski PJ, Jordan DW, et al. Image quality and diagnostic performance of a digital PET prototype in patients with oncologic diseases: initial experience and comparison with analog PET. J Nucl Med. 2015;56:1378–85. https://doi.org/10.2967/jnumed.114.148338.
13. van Sluis J, Boellaard R, Dierckx RA, Stormezand G, Glaudemans A, Noordzij W. Image quality and activity optimization in oncological (18)F-FDG PET using the digital Biograph Vision PET/CT. J Nucl Med. 2019. https://doi.org/10.2967/jnumed.119.234351.
14. Lopez-Mora DA, Flotats A, Fuentes-Ocampo F, Camacho V, Fernandez A, Ruiz A, et al. Comparison of image quality and lesion detection between digital and analog PET/CT. Eur J Nucl Med Mol Imaging. 2019;46:1383–90. https://doi.org/10.1007/s00259-019-4260-z.
15. Afshar-Oromieh A, Debus N, Uhrig M, Hope TA, Evans MJ, Holland-Letz T, et al. Impact of long-term androgen deprivation therapy on PSMA ligand PET/CT in patients with castration-sensitive prostate cancer. Eur J Nucl Med Mol Imaging. 2018;45:2045–54. https://doi.org/10.1007/s00259-018-4079-z.
16. Eder M, Neels O, Muller M, Bauder-Wust U, Remde Y, Schafer M, et al. Novel preclinical and radiopharmaceutical aspects of [68Ga]Ga-PSMA-HBED-CC: a new PET tracer for imaging of prostate cancer. Pharmaceuticals (Basel). 7:779–96. https://doi.org/10.3390/ph7070779.
17. Fendler WP, Eiber M, Beheshti M, Bomanji J, Ceci F, Cho S, et al. (68)Ga-PSMA PET/CT: joint EANM and SNMMI procedure guideline for prostate cancer imaging: version 1.0. Eur J Nucl Med Mol Imaging. 2017;44:1014–24. https://doi.org/10.1007/s00259-017-3670-z.
18. Rischpler C, Beck TI, Okamoto S, Schlitter AM, Knorr K, Schwaiger M, et al. (68)Ga-PSMA-HBED-CC uptake in cervical, coeliac and sacral ganglia as an important pitfall in prostate cancer PET imaging. J Nucl Med. 2018. https://doi.org/10.2967/jnumed.117.204677.
19. Afshar-Oromieh A, Sattler LP, Steiger K, Holland-Letz T, da Cunha ML, Mier W, et al. Tracer uptake in mediastinal and paraaortal thoracic lymph nodes as a potential pitfall in image interpretation of PSMA ligand PET/CT. Eur J Nucl Med Mol Imaging. 2018;45:1179–87. https://doi.org/10.1007/s00259-018-3965-8.
20. Krohn T, Verburg FA, Pufe T, Neuhuber W, Vogg A, Heinzel A, et al. [(68)Ga]PSMA-HBED uptake mimicking lymph node metastasis in coeliac ganglia: an important pitfall in clinical practice. Eur J Nucl Med Mol Imaging. 2015;42:210–4. https://doi.org/10.1007/s00259-014-2915-3.
21. Afshar-Oromieh A, Vollnberg B, Alberts I, Bahler A, Sachpekidis C, Dijkstra L, et al. Comparison of PSMA-ligand PET/CT and multiparametric MRI for the detection of recurrent prostate cancer in the pelvis. Eur J Nucl Med Mol Imaging. 2019. https://doi.org/10.1007/s00259-019-04438-w.
22. Sawicki LM, Kirchner J, Buddensieck C, Antke C, Ullrich T, Schimmoller L, et al. Prospective comparison of whole-body MRI and (68)Ga-PSMA PET/CT for the detection of biochemical recurrence of prostate cancer after radical prostatectomy. Eur J Nucl Med Mol Imaging. 2019;46:1542–50. https://doi.org/10.1007/s00259-019-04308-5.
23. Calais J, Czernin J, Fendler WP, Elashoff D, Nickols NG. Randomized prospective phase III trial of (68)Ga-PSMA-11 PET/CT molecular imaging for prostate cancer salvage radiotherapy planning [PSMA-SRT]. BMC Cancer. 2019;19:18. https://doi.org/10.1186/s12885-018-5200-1.
24. Schillaci O, Urbano N. Digital PET/CT: a new intriguing chance for clinical nuclear medicine and personalized molecular imaging. Eur J Nucl Med Mol Imaging. 2019. https://doi.org/10.1007/s00259-019-04300-z.
25. Fuentes-Ocampo F, Lopez-Mora DA, Flotats A, Paillahueque G, Camacho V, Duch J, et al. Digital vs analog PET/CT: intra-subject comparison of the SUVmax in target lesions and reference regions European journal of nuclear medicine and molecular imaging 2019. doi:https://doi.org/10.1007/s00259-018-4256-0.
26. Sachpekidis C, Kopka K, Eder M, Hadaschik BA, Freitag MT, Pan L, et al. 68Ga-PSMA-11 Dynamic PET/CT Imaging in Primary Prostate Cancer. Clin Nucl Med. 2016;41:e473–e9. https://doi.org/10.1097/RLU.0000000000001349.
27. Afshar-Oromieh A, Hetzheim H, Kubler W, Kratochwil C, Giesel FL, Hope TA, et al. Radiation dosimetry of (68)Ga-PSMA-11 (HBED-CC) and preliminary evaluation of optimal imaging timing. Eur J Nucl Med Mol Imaging. 2016;43:1611–20. https://doi.org/10.1007/s00259-016-3419-0.
28. Rauscher I, Kronke M, Konig M, Gafita A, Maurer T, Horn T, et al. Matched-pair comparison of (68)Ga-PSMA-11 and (18)F-PSMA-1007 PET/CT: frequency of pitfalls and detection efficacy in biochemical recurrence after radical prostatectomy. J Nucl Med. 2019. https://doi.org/10.2967/jnumed.119.229187.
29. Paschalis A, Sheehan B, Riisnaes R, Rodrigues DN, Gurel B, Bertan C, et al. Prostate-specific membrane antigen heterogeneity and DNA repair defects in prostate cancer. Eur Urol. 2019;76:469–78. https://doi.org/10.1016/j.eururo.2019.06.030.
30. Hubble D, Robins P. RE: Uptake in sympathetic ganglia on 68Ga-PSMA-HBED PET/CT: A potential pitfall in scan interpretation. J

Med Imaging Radiat Oncol. 2018;62:377–8. https://doi.org/10.1111/1754-9485.12739.

31. Kanthan GL, Hsiao E, Vu D, Schembri GP. Uptake in sympathetic ganglia on 68Ga-PSMA-HBED PET/CT: a potential pitfall in scan interpretation. J Med Imaging Radiat Oncol. 2017;61:732–8. https://doi.org/10.1111/1754-9485.12622.
32. Rahbar K, Afshar-Oromieh A, Bogemann M, Wagner S, Schafers M, Stegger L, et al. (18)F-PSMA-1007 PET/CT at 60 and 120 minutes in patients with prostate cancer: biodistribution, tumour detection and activity kinetics. Eur J Nucl Med Mol Imaging. 2018;45:1329–34. https://doi.org/10.1007/s00259-018-3989-0.
33. van der Vos CS, Koopman D, Rijnsdorp S, Arends AJ, Boellaard R, van Dalen JA, et al. Quantification, improvement, and harmonization of small lesion detection with state-of-the-art PET. Eur J Nucl Med Mol Imaging. 2017;44:4–16. https://doi.org/10.1007/s00259-017-3727-z.
34. Koopman D, Jager PL, van Dalen JA. Small-voxel reconstructions significantly influence SUVs in PET imaging. Eur J Nucl Med Mol Imaging. 2019;46:1751–2. https://doi.org/10.1007/s00259-019-04301-y.